RSC Advances

PAPER

View Article Online
View Journal | View Issue

Cite this: *RSC Adv.*, 2017, **7**, 43831

Facile preparation and excellent microwave absorption properties of an RGO/$Co_{0.33}Ni_{0.67}$ lightweight absorber

Hai Pan, Mingzhen Xu, Qing Qi and Xiaobo Liu*

Novel microwave absorbers combining $Co_{0.33}Ni_{0.67}$ alloy and reduced graphene oxide (RGO) are fabricated and their excellent microwave absorption properties demonstrated. $Co_{0.33}Ni_{0.67}$ alloy particles are prepared by a one-pot solvent-thermal method from $CoCl_2 \cdot 6H_2O$ and $NiCl_2 \cdot 6H_2O$. The prepared $Co_{0.33}Ni_{0.67}$ alloy particles are confirmed from SEM observation, EDS analysis and XRD measurements. RGO/$Co_{0.33}Ni_{0.67}$ composites are then fabricated by adding the $Co_{0.33}Ni_{0.67}$ alloy particles into a colloidal dispersion of GO and thermally reducing at 210 °C. The composition of RGO/$Co_{0.33}Ni_{0.67}$ is characterized by Raman, XPS, VSM, XRD and FTIR measurements. An SEM micrograph indicates the sandwich-like structure of RGO/$Co_{0.33}Ni_{0.67}$ with $Co_{0.33}Ni_{0.67}$ alloy particles intercalated into the RGO sheets. By suitably adjusting the dielectric loss and magnetic loss derived from different contents of the RGO and $Co_{0.33}Ni_{0.67}$, an RGO/$Co_{0.33}Ni_{0.67}$ composite with excellent microwave absorption properties is obtained. The maximum reflection loss is up to −50 dB at a thickness of only 1.8 mm. In addition, the absorption bandwidth exceeding −10 dB reaches up to 14.0 GHz with matching thicknesses of 5.0–1.4 mm and covers the whole Ku band at a thickness of only 2.0 mm.

Received 20th June 2017
Accepted 5th September 2017

DOI: 10.1039/c7ra06849b

rsc.li/rsc-advances

1. Introduction

Electromagnetic interference and irradiation derived from electromagnetic waves have recently become a serious problem with the development of phones, computers and other electronic devices. As a result, microwave absorbing materials have attracted extensive attentions not only for their wide applications in military, industrial and civil fields, but also for their significant roles in protecting the environment and health of human beings. According to the literature,[1–4] the absorption mechanism of microwave absorbing materials is due to energy conversion, that is, the energy of the incident wave is converted into other forms of energy (*e.g.* heat energy). This energy conversion can be caused by magnetic loss and dielectric loss of the microwave absorbing material, which are expressed by the complex permeability and complex permittivity, respectively. Many magnetic loss materials and dielectric loss materials have been fabricated and their microwave absorption properties investigated.[5–8] However, to improve the ability of electromagnetic absorption, an excellent impedance matching of magnetic loss and dielectric loss should be achieved.

The ideal microwave absorbers possess characteristics of low density, thin, wide frequency adsorption band and strong adsorption. Ferrites as the traditional absorbing material have characteristics of strong adsorption, while their applications are limited owe to the high density and narrow absorbing band.[9–12] Incorporating the magnetic-particle into the polymeric and/or carbon-based materials is an efficient method to obtain new absorber with low density and high reflection loss.[13–15] Graphene, as a novel carbon-based material has been widely studied due to its unique merit including high dielectric loss and low density.[16–19] However, as a nonmagnetic material, the microwave absorption property of graphene is mostly attributed to its dielectric loss, resulting in poor impedance matching.[20] Hence, many graphene/magnetic-particle composites have been fabricated to improve microwave absorption property, such as RGO/Fe_3O_4,[21] RGO/Co_3O_4,[22] RGO/$MnFe_2O_4$/PVDF[23] and so on. However, to the best of our knowledge, no report on microwave absorbing material based on graphene and $Co_{0.33}Ni_{0.67}$ alloy has been published so far.

In this work, sandwich-like RGO/$Co_{0.33}Ni_{0.67}$ composite as microwave absorber was fabricated by a simple one-pot solvent-thermal method and thermal reduction process. First, $Co_{0.33}Ni_{0.67}$ alloy particles was prepared by solvent-thermal method. Then, GO/$Co_{0.33}Ni_{0.67}$ composite was prepared from $Co_{0.33}Ni_{0.67}$ and GO through coordinate bond. Finally, RGO/$Co_{0.33}Ni_{0.67}$ composite was obtained by thermal reduction of the GO/$Co_{0.33}Ni_{0.67}$ composite at high temperature (210 °C). The prepared RGO/$Co_{0.33}Ni_{0.67}$ composite shows excellent absorption

Research Branch of Advanced Functional Materials, High Temperature Resistant Polymers and Composites Key Laboratory of Sichuan Province, School of Microelectronic and Solid-State Electronic, University of Electronic Science and Technology of China, Chengdu 610054, China. E-mail: liuxb@uestc.edu.cn; Tel: +86-28-83207326

property in comparison with $Co_{0.33}Ni_{0.67}$ alloy. The fabrication and characterization of the RGO/$Co_{0.33}Ni_{0.67}$ composites are given and the mechanism of the electromagnetic characteristics of the obtained materials is studied and discussed.

2. Experimental

2.1 Synthesis of $Co_{0.33}Ni_{0.67}$ alloy and graphene oxide (GO)

$Co_{0.33}Ni_{0.67}$ alloy particles were prepared by a one-pot solvent-thermal method as follow: $CoCl_2 \cdot 6H_2O$ (2.5 mmol), $NiCl_2 \cdot 6H_2O$ (10 mmol), $CH_3COONa \cdot 3H_2O$ (0.1 mol) and PEG2000 (2 mmol) were dissolved in EG (160 mL) solution at 60 °C with mechanical stirring for 10 min and then the mixed solution was poured into a Teflon-lined stainless-steel autoclave. The autoclave was sealed and heated at 200 °C for 15 h. The product was separated and washed several times with distilled water and ethanol, dried at 80 °C for 8 h. GO was fabricated according to the ref. 24.

2.2 Preparation of RGO/$Co_{0.33}Ni_{0.67}$ composites

A certain amount of $Co_{0.33}Ni_{0.67}$ particles was added into a three-necked flask containing GO colloidal dispersion (15 mg mL^{-1}). The mass ratios of GO and $Co_{0.33}Ni_{0.67}$ are 100/200 mg, 150/150 mg and 200/100 mg (defined as GO/$Co_{0.33}Ni_{0.67}$-1/2, GO/$Co_{0.33}Ni_{0.67}$-1/1 and GO/$Co_{0.33}Ni_{0.67}$-2/1), respectively. Then GO/$Co_{0.33}Ni_{0.67}$ colloidal dispersion was stirred for 3 h within an ultrasonic bath. After that the GO/$Co_{0.33}Ni_{0.67}$ colloidal dispersion was poured on a clean glass plate and dried at 80 °C overnight. The dried samples were further thermally reduced at 210 °C for 6 h yielding RGO/$Co_{0.33}Ni_{0.67}$ composites with a flaky appearance.

2.3 Characterization

Thermal gravimetric analysis (TGA) was carried out under a nitrogen atmosphere using a TA Instruments TGA-Q50 at a heating rate of 20 °C min^{-1} and a purge of 40 mL min^{-1}. X-ray diffraction (XRD) tests of all samples were recorded using a RINT 2400 vertical goniometer (Rigaku, Japan) with Cu Kα radiation. The morphology of the products was observed by a scanning electron microscopic (SEM, JSM6490LV, Japan). The elemental composition was detected by energy dispersive spectrometer (EDS) spectrum deriving from the SEM. X-ray photoelectron spectroscopic (XPS) was measured on an ESCA 2000 (VG Microtech, UK) using a monochromic Al Kα ($h\nu$ = 1486.6 eV) X-ray source. The microwave absorption properties of the $Co_{0.33}Ni_{0.67}$ alloy and RGO/$Co_{0.33}Ni_{0.67}$ composites were investigated by electromagnetic (EM) parameters which were tested by a vector network analyzer (HP8722ES). For the EM measurement, the sample preparation is as follows: the flaky RGO/$Co_{0.33}Ni_{0.67}$ composite is cut into round pieces, stacked on a layer by layer and mixed with melted paraffin by mass ratio of 1 : 1. The mixture is placed into the mold until the paraffin solidified, and then compressed into a circular ring shapes (outer diameter: 7.0 mm, inner diameter: 3.0 mm, thickness: 3.0 mm). The prepared circular ring is mounted on a fixture linking a vector network analyzer for EM parameter testing.

3. Results and discussion

$Co_{0.33}Ni_{0.67}$ alloy particles are prepared by a one-pot solvent-thermal method and characterized by SEM, EDS and XRD. The SEM and EDS images of the as-synthesized $Co_{0.33}Ni_{0.67}$ alloy particles are shown in the Fig. 1(a and b). $Co_{0.33}Ni_{0.67}$ shows near-spherical structure in the SEM image. The EDS spectrum indicates that the $Co_{0.33}Ni_{0.67}$ is composed of 67 mol% Ni and 33 mol% of Co and no other element is found, indicating the high purity of the as-synthesized $Co_{0.33}Ni_{0.67}$. On the XRD pattern (Fig. 1(c)), the main diffraction peaks of the $Co_{0.33}Ni_{0.67}$ are observed at $2\theta = 44.5°$, 51.9°, and 71.6° corresponding to the (111), (200) and (220) planes, respectively. This result is consistent with the standard XRD pattern of the $Co_{0.33}Ni_{0.67}$ with face-centered cubic structure (JCPDS no. 15-0806 and no. 04-0850). GO is fabricated strictly according to the reference. The sharp diffraction peak appeared at $2\theta = 10.5°$ on the XRD pattern corresponding to the (002) plane of graphite oxide. The GO sheets are stacked during the drying process. Therefore, the test sample shows the characteristic peak of the graphite oxide in the XRD pattern. The TGA and DTG curves of GO are given in the Fig. 1(d). The rapid weight loss between 180 °C and 230 °C on the TGA curve is observed, which is attribute to the removal of the oxygen-containing groups on the surface of GO. From the DTG curve, it can be observed that the fastest decomposition rate of GO is at 210 °C. Accordingly, GO could be effectively changed back to the reduced graphene oxide by thermal reduction at 210 °C.

The XPS analysis is employed to confirm the reduction of GO, as presented in the Fig. 2(a–c). From the Fig. 2(a), it is observed that the intensity ratio of the C 1s peak to O 1s peak of RGO is obviously higher than that of the GO, indicating the removal of oxygen-containing functional groups of the GO and the recovery of network structure of the sp^2 carbon (C=C/C–C, C1). In addition, the C 1s XPS spectra for GO and RGO/$Co_{0.33}Ni_{0.67}$ are shown in the Fig. 2(b and c). For GO, the peaks appeared at

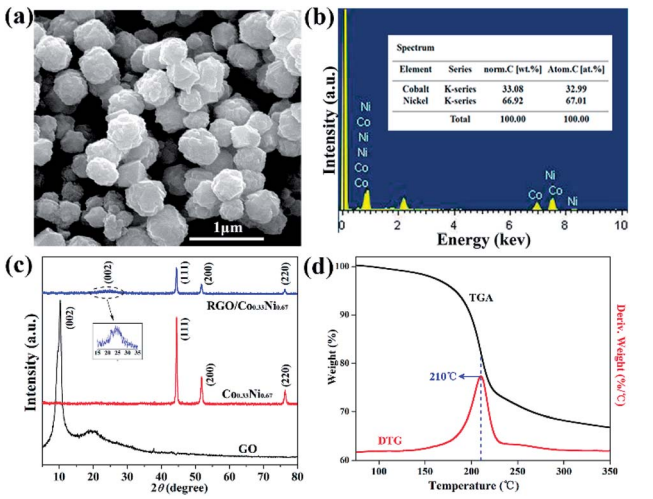

Fig. 1 (a) The SEM and (b) the EDS images of the pure $Co_{0.33}Ni_{0.67}$; (c) the XRD parameters of the GO, $Co_{0.33}Ni_{0.67}$ and RGO/$Co_{0.33}Ni_{0.67}$-1/1; (d) the TGA and DTG curves of the GO.

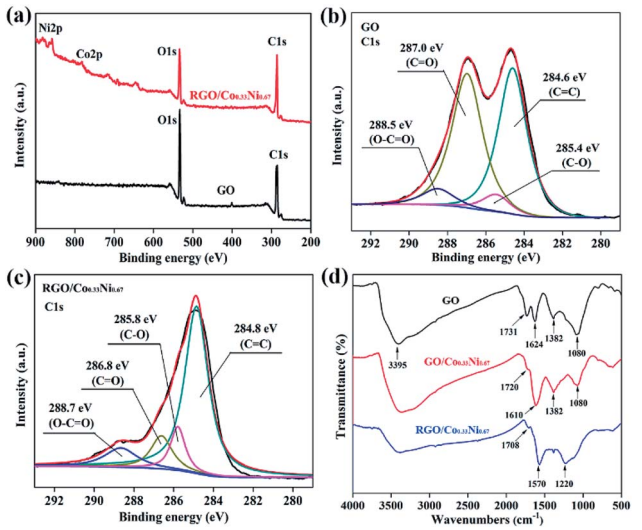

Fig. 2 (a) The XPS spectra of the GO and RGO/$Co_{0.33}Ni_{0.67}$; the C 1s XPS spectra of (b) the GO and (c) RGO/$Co_{0.33}Ni_{0.67}$; (d) the FTIR spectra of the GO, GO/$Co_{0.33}Ni_{0.67}$ and RGO/$Co_{0.33}Ni_{0.67}$.

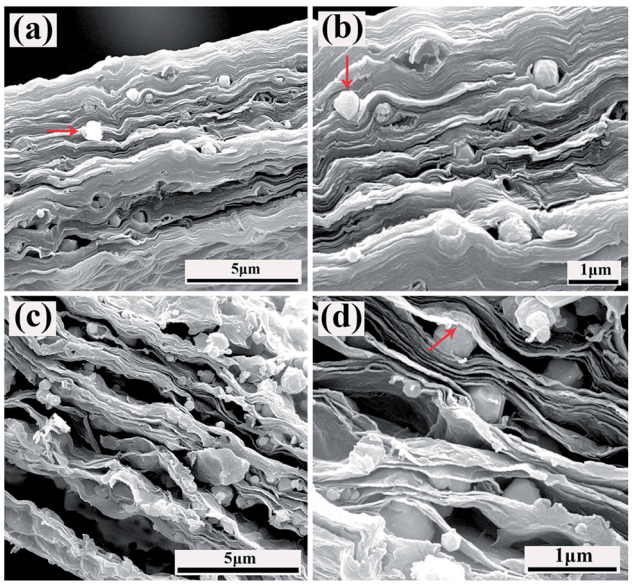

Fig. 3 (a, b) The SEM images of fracture surface of the GO/$Co_{0.33}Ni_{0.67}$-1/1; (c, d) the SEM images of fracture surface of the RGO/$Co_{0.33}Ni_{0.67}$-1/1.

284.6 eV, 285.4 eV, 287.0 eV, and 288.5 eV are assigned to the C=C/C–C bond, C–O bond (hydroxyl and epoxy), C=O bond (carbonyl), and O–C=O bond (carboxyl), respectively. Compared with the GO, it is clear that the peaks of the oxygen-containing functional groups for RGO/$Co_{0.33}Ni_{0.67}$ become observably weaker. According to the XPS results, it can be concluded that most of oxygen-containing functional groups of the GO are successfully removed, that is, the GO is efficiently reduced.

RGO/$Co_{0.33}Ni_{0.67}$ composites are fabricated by adding as-prepared $Co_{0.33}Ni_{0.67}$ into the colloidal dispersion of GO and thermally reducing at 210 °C. Instead of physical blending, the interaction between GO sheets and $Co_{0.33}Ni_{0.67}$ is coordination bond, which can be confirmed by FTIR analysis. In the Fig. 2(d), the characteristic peaks located at 3395, 1731, 1624, 1382 and 1080 cm^{-1} are assigned to the O–H stretching vibration, C=O stretching vibrations from carbonyl groups, C=C vibrations from the aromatic carbon, C–OH stretching vibrations and C–O vibrations from epoxy groups on GO, respectively.[25] However, for FTIR spectra of GO/$Co_{0.33}Ni_{0.67}$, the peak of C=O stretching vibrations situated at 1720 cm^{-1} disappears as compared to that of GO, indicating the formation of coordination bond between the carboxylic acid and $Co_{0.33}Ni_{0.67}$.[26] After the thermal reduction at 210 °C, most of the peaks of oxygen-containing functional groups on the FTIR spectra of RGO/$Co_{0.33}Ni_{0.67}$ disappear and new peaks appear at 1570 and 1220 cm^{-1} ascribing to the skeletal vibration of RGO sheets are observed, indicating the successful reduction of GO. In addition, the disappearance of the peak at $2\theta = 10.5°$ and the appearance of the broad diffraction peak located at $2\theta = 20–30°$ on the XRD pattern of RGO/$Co_{0.33}Ni_{0.67}$ (Fig. 1(c)) also confirmed the reduction of GO.[27]

Fig. 3 shows SEM images of fracture surface of the GO/$Co_{0.33}Ni_{0.67}$ and RGO/$Co_{0.33}Ni_{0.67}$. It is obvious to see the ordered sandwich-like structures with $Co_{0.33}Ni_{0.67}$ inserted into the multilayered GO in GO/$Co_{0.33}Ni_{0.67}$. After thermal reduction, $Co_{0.33}Ni_{0.67}$ is still lined in the multilayer of the RGO with the original appearance and morphology, as presented in the Fig. 3(c and d). In addition, for the GO/$Co_{0.33}Ni_{0.67}$ composite, it can be found that GO nanoplatelets are closely stacked layer by layer. Whereas a larger space distance is observed between different RGO nanoplatelets in the RGO/$Co_{0.33}Ni_{0.67}$ composite, caused by the gas generated during the thermal reduction process.

To investigate the microwave absorption properties of composites, the frequency dependence relative complex permittivity ($\varepsilon_r = \varepsilon' - j\varepsilon''$) and relative complex permeability ($\mu_r = \mu' - j\mu''$) of the $Co_{0.33}Ni_{0.67}$ and RGO/$Co_{0.33}Ni_{0.67}$ composites was measured and results are shown in Fig. 4(a–d). Generally, the storage capacity of electromagnetic energy can be expressed by the real permittivity (ε') and real permeability (μ'), whereas the energy dissipation and magnetic loss are associated to the imaginary permittivity (ε'') and imaginary permeability (μ''), respectively. As shown in Fig. 4(a), for the pure $Co_{0.33}Ni_{0.67}$, it can be found that the ε' value is approximately equal to 5.7 in the whole frequency range. For the RGO/$Co_{0.33}Ni_{0.67}$-1/2, the ε' value is lower than that of the pure $Co_{0.33}Ni_{0.67}$. With the increasing content of the RGO, the ε' value is higher than that of the pure $Co_{0.33}Ni_{0.67}$. As shown in Fig. 4(b), the ε'' value of the pure $Co_{0.33}Ni_{0.67}$ increases slowly in the whole frequency range, while the ε'' values of the RGO/$Co_{0.33}Ni_{0.67}$-1/2, RGO/$Co_{0.33}Ni_{0.67}$-1/1, and RGO/$Co_{0.33}Ni_{0.67}$-2/1 are higher than that of the pure $Co_{0.33}Ni_{0.67}$ over the whole test frequency range and decline with the increase of frequency. Compared with pure $Co_{0.33}Ni_{0.67}$, the RGO/$Co_{0.33}Ni_{0.67}$ composites exhibit higher values of the complex permittivity, which is attributed to the introduction of RGO. The presence of RGO can enhance electric conductivity and electric polarization of the composites system.

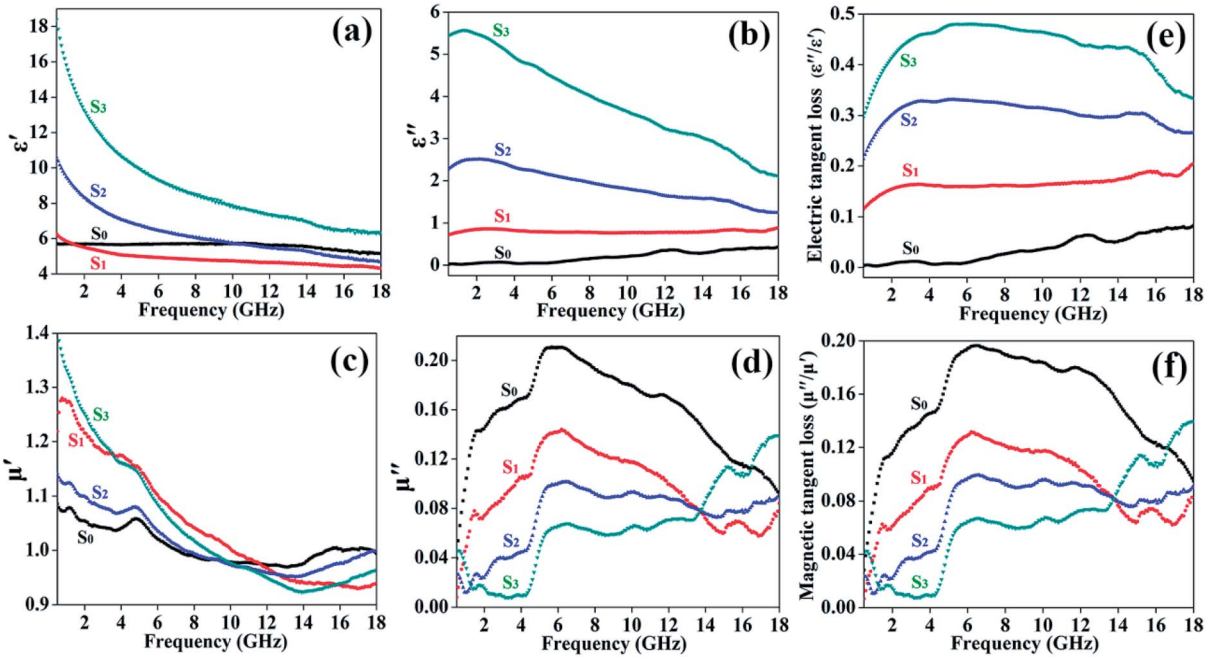

Fig. 4 Frequency dependence for (a) real and (b) imaginary parts of relative complex permittivity and (c) real and (d) imaginary parts of relative complex permeability of all samples; (e) electric and (f) magnetic tangent loss curves of all samples. (S_0): $Co_{0.33}Ni_{0.67}$; (S_1): RGO/$Co_{0.33}Ni_{0.67}$-1/2; (S_2): RGO/$Co_{0.33}Ni_{0.67}$-1/1; (S_3): RGO/$Co_{0.33}Ni_{0.67}$-2/1.

This can be explained by the free electron theory, $\varepsilon'' = 1/2\varepsilon_o\pi\rho f$, where f is the frequency of the electromagnetic wave, ρ is the resistivity and ε_o is the permittivity of the free space.[28–30] Owing to the presence of RGO with high conductivity, a conducting network is formed in the RGO/$Co_{0.33}Ni_{0.67}$ composites, resulting in the reduction of the resistivity and then the ε'' value increases. The improved complex permittivity of the RGO/$Co_{0.33}Ni_{0.67}$ composites is expected to enhance the microwave absorption property of composite.

As presented in Fig. 4(c), the μ' values of the RGO/$Co_{0.33}Ni_{0.67}$ composites are higher in the low frequency region (0.5 GHz to 11.0 GHz) and are lower in the high frequency region (11.0 GHz to 18.0 GHz) in comparison with that of the pure $Co_{0.33}Ni_{0.67}$. The μ'' curves of all samples are given in Fig. 4(d). The μ'' values of the RGO/$Co_{0.33}Ni_{0.67}$ composites are also lower than that of the pure $Co_{0.33}Ni_{0.67}$. For the pure $Co_{0.33}Ni_{0.67}$, the μ'' value declines gradually from 6.0 GHz to 18 GHz, while for the RGO/$Co_{0.33}Ni_{0.67}$ composites, the μ'' values show gradually increasing trend with increasing content of the RGO from 6.0 GHz to 18.0 GHz. From the μ'' curves of the RGO/$Co_{0.33}Ni_{0.67}$ composites, four resonance bands are found and the peak values occur at 1.5, 6.5, 10.0 and 15.2 GHz, respectively. Generally, these resonances will cause magnetic loss, which is expected to improve the microwave absorption of the RGO/$Co_{0.33}Ni_{0.67}$ composites.[15] Furthermore, the μ' values of all samples decrease with an increase in frequency, which is caused by the hysteresis effect of the ferromagnetic domain walls and magnetic induction intensity.[31]

As two important parameters for evaluating microwave absorption property, the dielectric tangent loss ($\tan\delta_\varepsilon = \varepsilon''/\varepsilon'$) and the magnetic tangent loss ($\tan\delta_\mu = \mu''/\mu'$) of all samples are shown in Fig. 4(e and f). It can be found that the $\tan\delta_\varepsilon$ values of the RGO/$Co_{0.33}Ni_{0.67}$ composites are improved in comparison with that of the pure $Co_{0.33}Ni_{0.67}$, whereas the $\tan\delta_\mu$ values are weakened, indicating that the introduction of RGO is promising for the increase of the dielectric loss rather than the magnetic loss. From Fig. 4(e and f), it also can be concluded that the $\tan\delta_\mu$ value of the pure $Co_{0.33}Ni_{0.67}$ is higher than its $\tan\delta_\varepsilon$ value, revealing that the main loss mechanism for the pure $Co_{0.33}Ni_{0.67}$ is magnetic loss. In contrast, the $\tan\delta_\varepsilon$ values of the RGO/$Co_{0.33}Ni_{0.67}$ composites are higher than their $\tan\delta_\mu$ values, demonstrating that the dielectric loss is regarded as the main loss mechanism after combining with RGO.[32]

The dielectric loss usually derives from nature resonance, electronic polarization and electronic conductivity.[26,33] For the RGO/$Co_{0.33}Ni_{0.67}$ composites, the $Co_{0.33}Ni_{0.67}$ and residual defects and groups of the RGO act as polarized scattering center which can absorb the electromagnetic energy.[33] As discussed above, according to the free electron theory, $\varepsilon'' = 1/2\varepsilon_o\pi\rho f$, the increase of ε'' values of the RGO/$Co_{0.33}Ni_{0.67}$ composites results in the enhancement of the dielectric loss, which is in favor of the improvement of electromagnetic absorption performance. Furthermore, the improved dielectric loss is also attributed to the 2D RGO nanosheets which can form a conducting network for dispersing charges since the 2D RGO nanosheets have the huge aspect ratio, layered structure and high conductivity.[15]

The magnetic loss roots in the nature resonance loss, the eddy current effect and anisotropic energy.[21,23,31,34] Since the $Co_{0.33}Ni_{0.67}$ is a ferromagnetic material, for the RGO/$Co_{0.33}Ni_{0.67}$ composites, the eddy current effect may be a significant factor to influence the microwave absorption property in the high frequency region. The eddy current loss can be express by the following equation:

$$\mu'' \approx 2\pi\mu_0(\mu')^2\sigma d^2 f/3 \quad (1)$$

$$C_0 = \mu''(\mu')^{-2}f^{-1} = 2\pi\mu_0\sigma d^2/3 \quad (2)$$

where σ is the electrical conductivity and μ_0 is the permeability in a vacuum. If the magnetic loss is caused by the eddy current loss, the C_0 value is equal to constant value as the change of frequency.[35] The C_0–f curves for all samples are given in Fig. 5. It can be seen that the C_0 value of the pure $Co_{0.33}Ni_{0.67}$ is reduced with the increase of frequency, whereas the C_0 values of the RGO/$Co_{0.33}Ni_{0.67}$ composites are almost constant in the frequency range of X to Ku band (8 GHz to 18 GHz), especially for the RGO/$Co_{0.33}Ni_{0.67}$-2/1 composite. These results reveal that the pure $Co_{0.33}Ni_{0.67}$ does not show obvious eddy current loss over the whole frequency range while the RGO/$Co_{0.33}Ni_{0.67}$ composites have an effective eddy current loss in the wide frequency range (8.0 to 18.0 GHz). Thus, the magnetic loss of the RGO/$Co_{0.33}Ni_{0.67}$ composites is mainly caused by the eddy current effect in the range of 8.0 GHz to 18.0 GHz. Moreover, the anisotropic energy (H_a) is another factor that results in the magnetic loss. The H_a value can be calculated by the following equation:

$$H_a = 4|K_1|/(3\mu_0 M_S) \quad (3)$$

where $|K_1|$ and M_S are the anisotropy coefficient and the saturation magnetization, respectively. The M_S value of the RGO/$Co_{0.33}Ni_{0.67}$ composites are much lower than that of the pure $Co_{0.33}Ni_{0.67}$, so the H_a value of the RGO/$Co_{0.33}Ni_{0.67}$ composites are higher than that of the $Co_{0.33}Ni_{0.67}$. The higher anisotropic energy is more beneficial to the enhancement of the microwave absorption property.[36,37]

Based on the transmit-line theory and the measured data of the relative complex permittivity and permeability, the microwave absorption property of the composites were investigated and the reflection loss (RL) of the electromagnetic wave was calculated by the following equation:

$$RL = 20\log_{10}|(Z_{in} - Z_0)/(Z_{in} + Z_0)| \quad (4)$$

$$Z_{in} = Z_0\sqrt{\frac{\mu_r}{\varepsilon_r}}\tanh\left[j\left(\frac{2f\pi d}{c}\right)\sqrt{\mu_r\varepsilon_r}\right] \quad (5)$$

where Z_{in} and Z_0 are the input impedance of absorber and the impedance of air, respectively. The μ_r and ε_r are the relative complex permeability and permittivity, respectively, and f is the frequency of the electromagnetic wave, d is the thickness of the absorbent and c is the velocity of light in vacuum.

Generally, the microwave absorption performance of materials can be evaluated by the reflection loss (RL) value. The RL values less than −10 dB and −20 dB imply more than 90.0% and 99.0% microwave absorption, respectively. Fig. 6 shows the theoretical RL values of all samples in the frequency range of 0.5 to 18.0 GHz with the matching thickness of 1.0–5.0 mm. It is clear that the microwave absorption performances of RGO/$Co_{0.33}Ni_{0.67}$ composite are enhanced with the increase of RGO loading and the matching thickness is reduced as the frequency increases. In addition, the absorption bands less than −10.0 dB shift toward lower frequency and thinner thickness. The results indicate that the RGO loading, test frequency and matching thickness have a significant influence on the microwave absorption performance. For pure $Co_{0.33}Ni_{0.67}$, the minimum RL value cannot reach −10.0 dB in the whole test frequency and thickness range, revealing that the pure $Co_{0.33}Ni_{0.67}$ cannot be used for practical application. For the RGO/$Co_{0.33}Ni_{0.67}$-1/1 composite, the RL value below −10.0 dB can be obtained between 5.0 GHz and 18.0 GHz with the matching thicknesses of 5.0–1.8 mm and the minimum RL value can reach up to −22.0 dB at 6.9 GHz with the thickness of 4.5 mm. For the RGO/$Co_{0.33}Ni_{0.67}$-2/1 composite, the RL value exceeding −10.0 dB can be adjusted between 4.0 to 18.0 GHz with the matching thicknesses of 5.0–1.4 mm and an outstanding RL value of −50.0 dB can be obtained at 16.0 GHz with the thickness of only 1.8 mm.

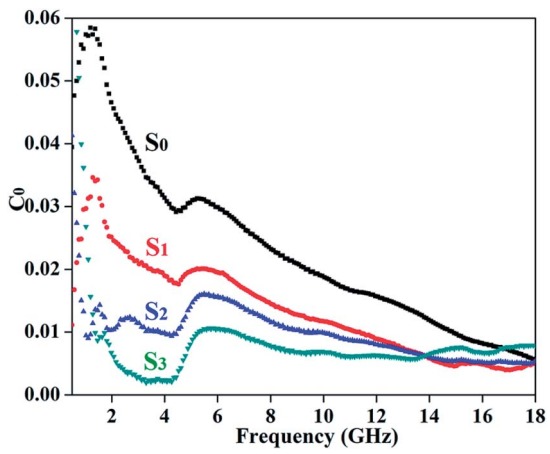

Fig. 5 The C_0–f curves of all samples. (S_0): $Co_{0.33}Ni_{0.67}$; (S_1): RGO/$Co_{0.33}Ni_{0.67}$-1/2; (S_2): RGO/$Co_{0.33}Ni_{0.67}$-1/1; (S_3): RGO/$Co_{0.33}Ni_{0.67}$-2/1.

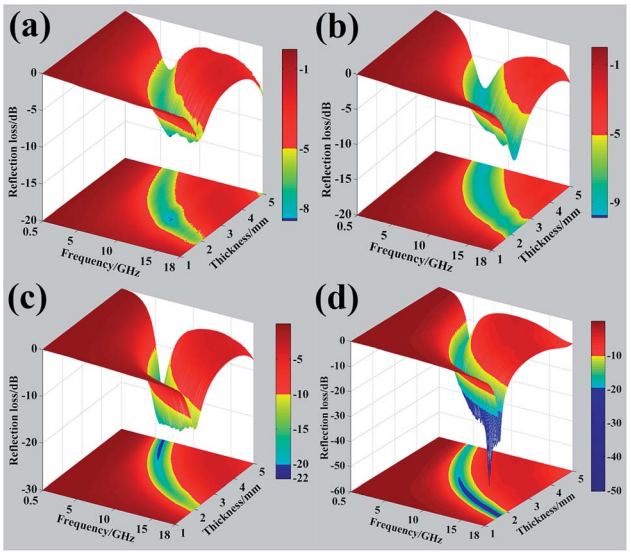

Fig. 6 The 3D reflection loss diagrams of (a) the pure $Co_{0.33}Ni_{0.67}$, (b) RGO/$Co_{0.33}Ni_{0.67}$-1/2, (c) RGO/$Co_{0.33}Ni_{0.67}$-1/1, and (d) RGO/$Co_{0.33}Ni_{0.67}$-2/1 with different matching thicknesses in the frequency range of 0.5 GHz to 18.0 GHz.

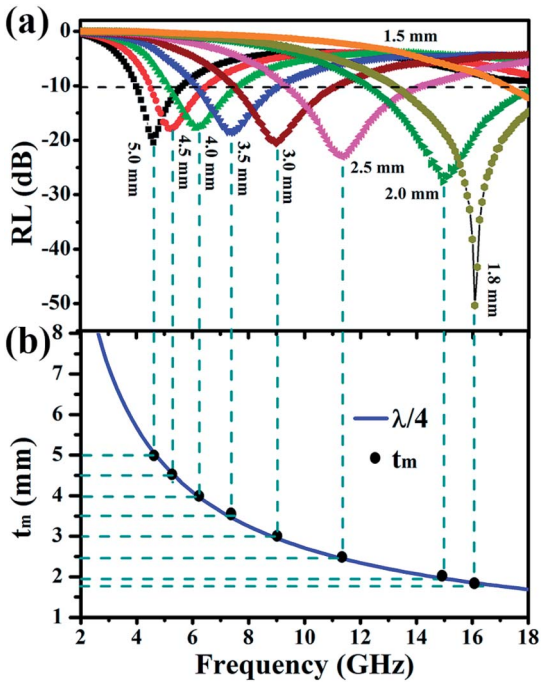

Fig. 7 (a) The reflection loss curves of the RGO/$Co_{0.33}Ni_{0.67}$-2/1 composite at different matching thicknesses; (b) the simulation curve of the quarter-wavelength matching model.

In addition, the absorption bandwidth (below −20.0 dB) of the RGO/$Co_{0.33}Ni_{0.67}$-2/1 composite is up to 9.8 GHz from 8.2 to 18.0 GHz with the matching thicknesses of 3.2–1.7 mm. It can be concluded that the RGO/$Co_{0.33}Ni_{0.67}$ composites possessed wider absorption bandwidth for the reflection loss below −10.0 dB in the range of C to Ku band (4.0–18.0 GHz), which makes it possible for application in civil devices, military radar and direct broadcast satellite.[38] Moreover, the absorption band under −10.0 dB is analogous to the curve of the quarter-wavelength matching model which expounds the relationship between the matching thickness (t_m) and the peak frequency (f_m) and can further explain possible mechanism resulting in the improvement of the microwave absorption performance.[39] The model can be expressed by the following equation:

$$f_m = nc \Big/ \left(4t_m \sqrt{|\mu_r||\varepsilon_r|}\right) \quad (6)$$

where $|\mu_r|$ and $|\varepsilon_r|$ are the modulus of the relative complex permeability and permittivity at f_m, respectively. On basis of the quarter-wavelength matching model, the reflected wave derived from the upper interface (the air-absorber) and the bottom interface (the absorber-metal plate) have inverse phase angle of 180°, giving rise to the cancellation of each other at the upper interface. The RL curves as a function of frequency for the RGO/$Co_{0.33}Ni_{0.67}$-2/1 composite with different matching thicknesses is shown in Fig. 7(a). According to the quarter-wavelength ($\lambda/4$) matching equation, a simulation curve of the matching

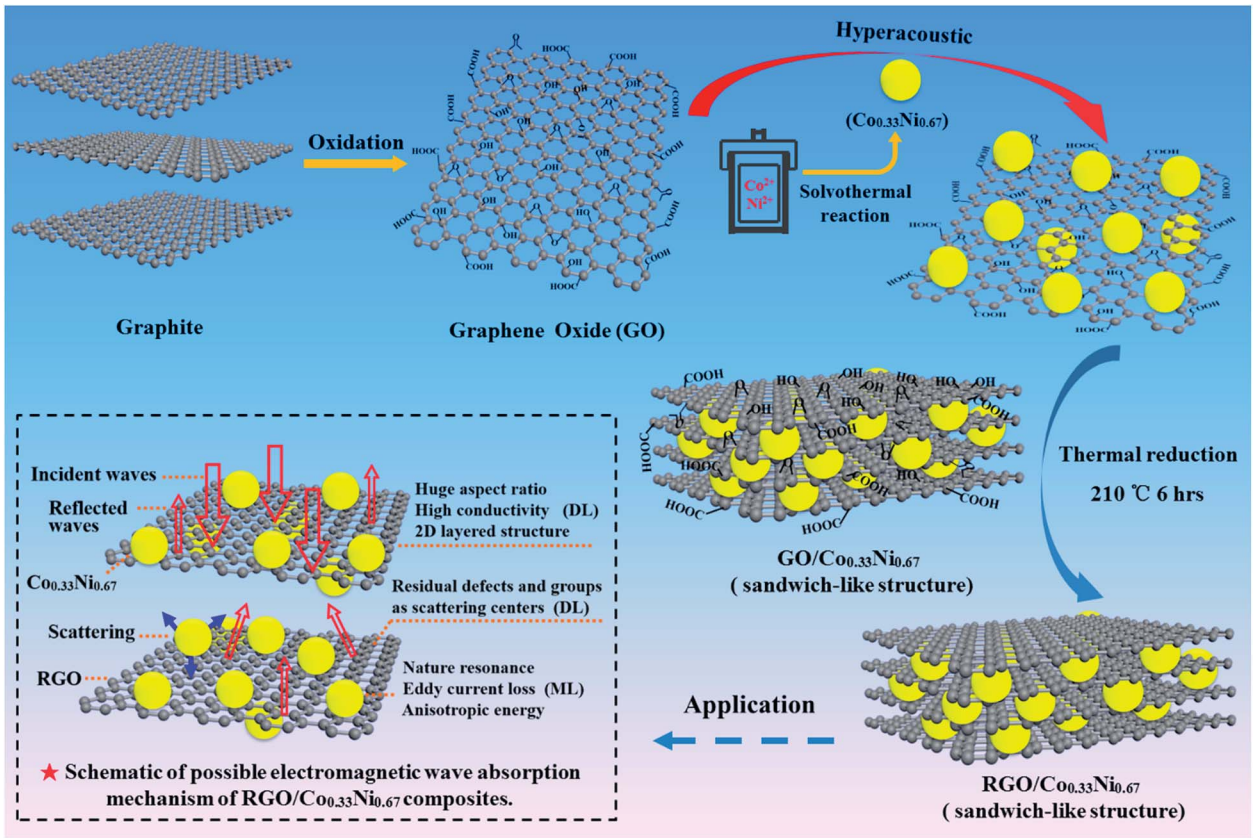

Scheme 1 The fabrication route and possible electromagnetic wave absorption mechanism of the RGO/$Co_{0.33}Ni_{0.67}$ composites.

thickness *versus* peak frequency is described in Fig. 7(b). In Fig. 7(a), the matching thickness *versus* frequency of the maximum absorption peak can be found on the simulation curve in Fig. 7(b), indicating that the experimental thickness and test frequency agree well with those of simulation curve. Moreover, it can be found that the absorption bandwidth below −10 dB covers the whole Ku band at a thickness of 2.0 mm. It can also be speculated that when the thickness of the absorber is under 1.5 mm, the peak frequency surpasses 18.0 GHz, revealing that the RGO/$Co_{0.33}Ni_{0.67}$ composites can be used at higher frequency and possess a thinner thickness.

4. Conclusions

In conclusion, the RGO/$Co_{0.33}Ni_{0.67}$ composites with ordered sandwich-like structure were synthesized by a simple one-pot solvent-thermal method and thermal reduction process at 210 °C. The prepared RGO/$Co_{0.33}Ni_{0.67}$ composites exhibited excellent microwave absorption properties. Particularly, for the RGO/$Co_{0.33}Ni_{0.67}$-2/1 composite, the maximum reflection loss is up to −50 dB at a thickness of only 1.8 mm, the absorption bandwidths for reflection loss below −10 dB and −20 dB reach up to 14.0 GHz (from 4.0 to 18.0 GHz) and 9.8 GHz (from 8.2 to 18.0 GHz) with the matching thicknesses of 5.0–1.4 mm and 3.2–1.7 mm, respectively. Due to the effective adjustment between dielectric loss and magnetic loss, the incident wave can be absorbed and dissipated efficiently, resulting in the enhancement of microwave absorption properties of RGO/$Co_{0.33}Ni_{0.67}$ composites. The dielectric loss is attributed to two aspects: (1) the 2D RGO nanosheets with the huge aspect ratio, layered structure and high conductivity; (2) the residual defects and groups attached to RGO as polarized scattering center. Magnetic loss results from the nature resonance loss, the eddy current effect and anisotropic energy. Based on above statement, a possible electromagnetic wave absorption mechanism of the RGO/$Co_{0.33}Ni_{0.67}$ composites is shown in Scheme 1. In this paper, the prepared RGO/$Co_{0.33}Ni_{0.67}$ composites possess light weight, strong reflection loss, and broadband absorption, which makes it possible for practical applications as high-performance microwave absorbers.

Conflicts of interest

There are no conflicts to declare.

Acknowledgements

The authors wish to thank for financial support of this work from the National Natural Science Foundation (No. 51373028, 51403029) and South Wisdom Valley Innovative Research Team Program and Ningbo Major (key) Science and Technology Research Plan (2013B06011).

Notes and references

1 T. Xia, C. Zhang, N. A. Oyler and X. Chen, *Adv. Mater.*, 2013, **25**, 6905–6910.
2 G. Sun, B. Dong, M. Cao, B. Wei and C. Hu, *Chem. Mater.*, 2011, **23**, 1587–1593.
3 S. Motojima, Y. Noda, S. Hoshiya and Y. Hishikawa, *J. Appl. Phys.*, 2003, **94**, 2325.
4 A. Zhang, M. Tang, X. Cao, Z. Lu and Y. Shen, *J. Mater. Sci.*, 2014, **49**, 4629–4635.
5 R. B. Yang, P. M. Reddy, C. J. Chang, P. A. Chen, J. K. Chen and C. C. Chang, *Chem. Eng. J.*, 2016, **285**, 497–507.
6 S. He, G. S. Wang, C. Lu, J. Liu, B. Wen, H. Liu, L. Guo and M. S. Cao, *J. Mater. Chem. A*, 2013, **1**, 4685.
7 C. Wang, X. Han, P. Xu, J. Wang, Y. Du, X. Wang, W. Qin and T. Zhang, *J. Phys. Chem. C*, 2010, **114**, 3196–3203.
8 L. Deng and M. Han, *Appl. Phys. Lett.*, 2007, **91**, 023119.
9 P. Akcora, H. Liu, S. K. Kumar, J. Moll, Y. Li, B. C. Benicewicz, L. S. Schadler, D. Acehan, A. Z. Panagiotopoulos, V. Pryamitsyn, V. Ganesan, J. Ilavsky, P. Thiyagarajan, R. H. Colby and J. F. Douglas, *Nat. Mater.*, 2009, **8**, 354–359.
10 S. Ni, S. Lin, Q. Pan, F. Yang, K. Huang and D. He, *J. Phys. D: Appl. Phys.*, 2009, **42**, 055004.
11 D. L. Zhao, Q. Lv and Z. M. Shen, *J. Alloys Compd.*, 2009, **480**, 634–638.
12 V. Sunny, P. Kurian, P. Mohanan, P. A. Joy and M. R. Anantharaman, *J. Alloys Compd.*, 2010, **489**, 297–303.
13 S. Dong, F. Meng, Z. Wang, M. Feng, K. Jia and X. Liu, *J. Alloys Compd.*, 2014, **617**, 751–755.
14 F. Meng, R. Zhao, Y. Zhan, Y. Lei, J. Zhong and X. Liu, *Appl. Surf. Sci.*, 2011, **257**, 5000–5006.
15 X. Li, J. Feng, Y. Du, J. Bai, H. Fan, H. Zhang, Y. Peng and F. Li, *J. Mater. Chem. A*, 2015, **3**, 5535–5546.
16 H. Guo, Y. Zhan, Z. Chen, F. Meng, J. Wei and X. Liu, *J. Mater. Chem. A*, 2013, **1**, 2286–2296.
17 K. S. Novoselov, A. K. Geim, S. V. Morozov, D. Jiang, Y. Zhang, S. V. Dubonos, I. V. Grigorieva and A. A. Firsov, *Science*, 2004, **306**, 666–669.
18 D. A. Dikin, S. Stankovich, E. J. Zimney, R. D. Piner, G. H. Dommett, G. Evmenenko, S. T. Nguyen and R. S. Ruoff, *Nature*, 2007, **448**, 457–460.
19 Y. Zhu, S. Murali, W. Cai, X. Li, J. W. Suk, J. R. Potts and R. S. Ruoff, *Adv. Mater.*, 2010, **22**, 3906–3924.
20 C. Wang, X. Han, P. Xu, X. Zhang, Y. Du, S. Hu, J. Wang and X. Wang, *Appl. Phys. Lett.*, 2011, **98**, 072906.
21 M. Zong, Y. Huang, Y. Zhao, X. Sun, C. Qu, D. Luo and J. Zheng, *RSC Adv.*, 2013, **3**, 23638.
22 P. B. Liu, Y. Huang and X. Sun, *ACS Appl. Mater. Interfaces*, 2013, **5**, 12355–12360.
23 X. J. Zhang, G. S. Wang, W. Q. Cao, Y. Z. Wei, J. F. Liang, L. Guo and M. S. Cao, *ACS Appl. Mater. Interfaces*, 2014, **6**, 7471–7478.
24 D. C. Marcano, D. V. Kosynkin, J. M. Berlin, A. Sinitskii, Z. Sun, A. Slesarev, L. B. Alemany, W. Lu and J. M. Tour, *ACS Nano*, 2010, **4**, 4806–4814.
25 S. Park, J. An, I. Jung, R. D. Piner, S. J. An, X. Li, A. Velamakanni and R. S. Ruoff, *Nano Lett.*, 2009, **9**, 1593–1597.
26 Y. T. Liu, M. Dang, X. M. Xie, Z. F. Wang and X. Y. Ye, *J. Mater. Chem.*, 2011, **21**, 18723.

27 O. K. Park, N. H. Kim, G. H. Yoo, K. Y. Rhee and J. H. Lee, *Composites, Part B*, 2010, **41**, 2–7.
28 Y. J. Chen, G. Xiao, T. S. Wang, Q. Y. Ouyang, L. H. Qi, Y. Ma, P. Gao, C. L. Zhu, M. S. Cao and H. B. Jin, *J. Phys. Chem. C*, 2011, **115**, 13603–13608.
29 B. Zhao, G. Shao, B. Fan, W. Zhao, Y. Xie and R. Zhang, *J. Mater. Chem. A*, 2015, **3**, 10345–10352.
30 R. Tamura, E. Lim, T. Manaka and M. Iwamoto, *J. Appl. Phys.*, 2006, **100**, 114515.
31 Q. Liu, X. Xu, W. Xia, R. Che, C. Chen, Q. Cao and J. He, *Nanoscale*, 2015, **7**, 1736–1743.
32 C. Wang, S. Hu, X. Han, W. Huang and L. Tian, *PLoS One*, 2013, **8**, e55928.
33 D. Chen, G. S. Wang, S. He, J. Liu, L. Guo and M. S. Cao, *J. Mater. Chem. A*, 2013, **1**, 5996.
34 P. J. V. D. Zaag, *J. Magn. Magn. Mater.*, 1999, **196–197**, 315–319.
35 H. Wang, Y. Dai, W. Gong, D. Geng, S. Ma, D. Li, W. Liu and Z. Zhang, *Appl. Phys. Lett.*, 2013, **102**, 223113.
36 J. Guo, X. Wang, P. Miao, X. Liao, W. Zhang and B. Shi, *J. Mater. Chem.*, 2012, **22**, 11933.
37 C. L. Zhu, M. L. Zhang, Y. J. Qiao, G. Xiao, F. Zhang and Y. J. Chen, *J. Phys. Chem. C*, 2010, **114**, 16229–16235.
38 X. Li, H. Yi, J. Zhang, J. Feng, F. Li, D. Xue, H. Zhang, Y. Peng and N. J. Mellors, *J. Nanopart. Res.*, 2013, **15**, 1472.
39 R. Li, T. Wang, G. Tan, W. Zuo, J. Wei, L. Qiao and F. Li, *J. Alloys Compd.*, 2014, **586**, 239–243.